Pergamon

PII: S0191-8141(97)00051-5

*Journal of Structural Geology*, Vol. 20, No. 1, pp. 77 to 92, 1998

0191-8141/98 $19.00 + 0.00

# Taylor-mill analogues for patterns of flow and deformation in rocks

RUUD WEIJERMARS

Department of Earth Sciences, King Fahd University of Petroleum and Minerals, Box 5070, 312 61 Dhahran, Saudi Arabia

(*Received* 27 *August* 1996; *accepted in revised form* 5 *June* 1997)

**Abstract**—The Giesekus design of Taylor's four-roll mill has been restored and is here used in novel flow visualizations of both pulsating and monotonously increasing strains. The particle movement paths and progressive deformation patterns visualized in these physical experiments are in agreement with those previously calculated analytically and constructed graphically. The progressive deformation of passive material markers is guided by flowlines. Circular flowlines accommodate rigid-body rotations without deformation. Elliptical flowlines result in pulsating strains. The maximum strain occurs when material particles, which were initially at the short axis of the elliptical flowlines, reach the long axis of the flow patterns. Monotonically increasing strains occur when flowlines are hyperbolic. The insight thus gained is extrapolated to suggest practical methods and assumptions that allow the reconstruction of particle movement paths from deformation features commonly observed in rocks. © 1998 Published by Elsevier Science Ltd.

## INTRODUCTION

Ductile deformation structures observed in rocks may be studied quantitatively by mapping the regional distribution of finite strain patterns. The formation of such strain patterns is the result of the relative movement of rock particles. Better knowledge of the particle movements would be useful because of the theoretical relationship between the flow patterns, the stress orientation and the direction of boundary displacement as discussed in detail elsewhere (Weijermars, 1993a). The problem with finding particle displacement paths or streamlines that guided the deformation patterns exposed in rocks is that stress orientation, direction of boundary displacement and particle movement paths themselves are commonly not preserved. Therefore, it is important to investigate how strain patterns relate to particle movement paths or streamlines in theory and experiment. This provides techniques to constrain the approximate orientation of the streamlines that may have led to the deformation patterns recorded in rocks. A new contribution to such attempts is briefly outlined here. The methods and approach followed are complementary to related work by Passchier and Simpson (1986), Masuda and Ando (1988), Hanmer and Passchier (1991), Simpson and De Paor (1993), Jiang and White (1995), Masuda *et al.* (1995a,b) and Tikoff and Fossen (1995).

Graphically, homogeneous deformation in planar flows can be represented by the progressive distortion of a passive unit circle into ellipses of increasing axial ratios. Physically, the progressive deformation of such strain circles is controlled by the particle movement paths. Theoretical investigations have demonstrated how hyperbolic flow patterns cause homogeneous deformation with progressive distortion of the strain ellipse (Ramberg, 1975a,b). The orientation of the principal stress axes and the relationships between finite strain, viscosity and strain rate have been elaborated for the full range of hyperbolic flow patterns (Weijermars, 1991). Another class of homogeneous deformation, distinguished on the basis of theoretical arguments, is controlled by elliptical streamlines which cause pulsating strains (Ramberg, 1975a,b). The rate of pulsation of the strain cycle can be quantified for competent inclusions using the viscosity contrast between the inclusion and the host rock, using various stress orientations (Weijermars, 1993b, 1997a).

Examples of homogeneous progressive deformation for both types of homogeneous flows (i.e. hyperbolic and elliptical) are illustrated qualitatively in Fig. 1. The occurrence of each particular flow pattern critically depends upon the kinematic vorticity number, a fluid mechanical number defined, for two-dimensional deformations, as the ratio of half the vorticity and the shear strain rate (Truesdell, 1953; Means *et al.*, 1980; Weijermars, 1991). In summary, monotonically increasing strains occur when $0 \leq W_k \leq 1$ and pulsating strains occur when $1 < W_k < \infty$. Limiting cases are pure shear ($W_k = 0$), simple shear ($W_k = 1$) and rigid-body rotation ($W_k = \infty$). Figure 2 illustrates quantitatively how the spectrum of flowlines for homogeneous plane strains is controlled by the values of (half the) vorticity and the strain rate.

Pure shear and simple shear boxes have been used extensively in scaled and unscaled models of mechanical instabilities with geological significance (folds, mullions, boudins, etc.). These shear boxes constrain the particle paths by the movement of the walls enclosing the model substance. An alternative approach constrains the particle movement paths using a Taylor mill comprising four rollers, a design made first by Sir Geoffrey Taylor, the late fluid mechanicist. The advantage of this approach is that a single apparatus allows modelling, not only of pure shear and simple shear deformations, but of all possible cases of plane, homogeneous deforma-

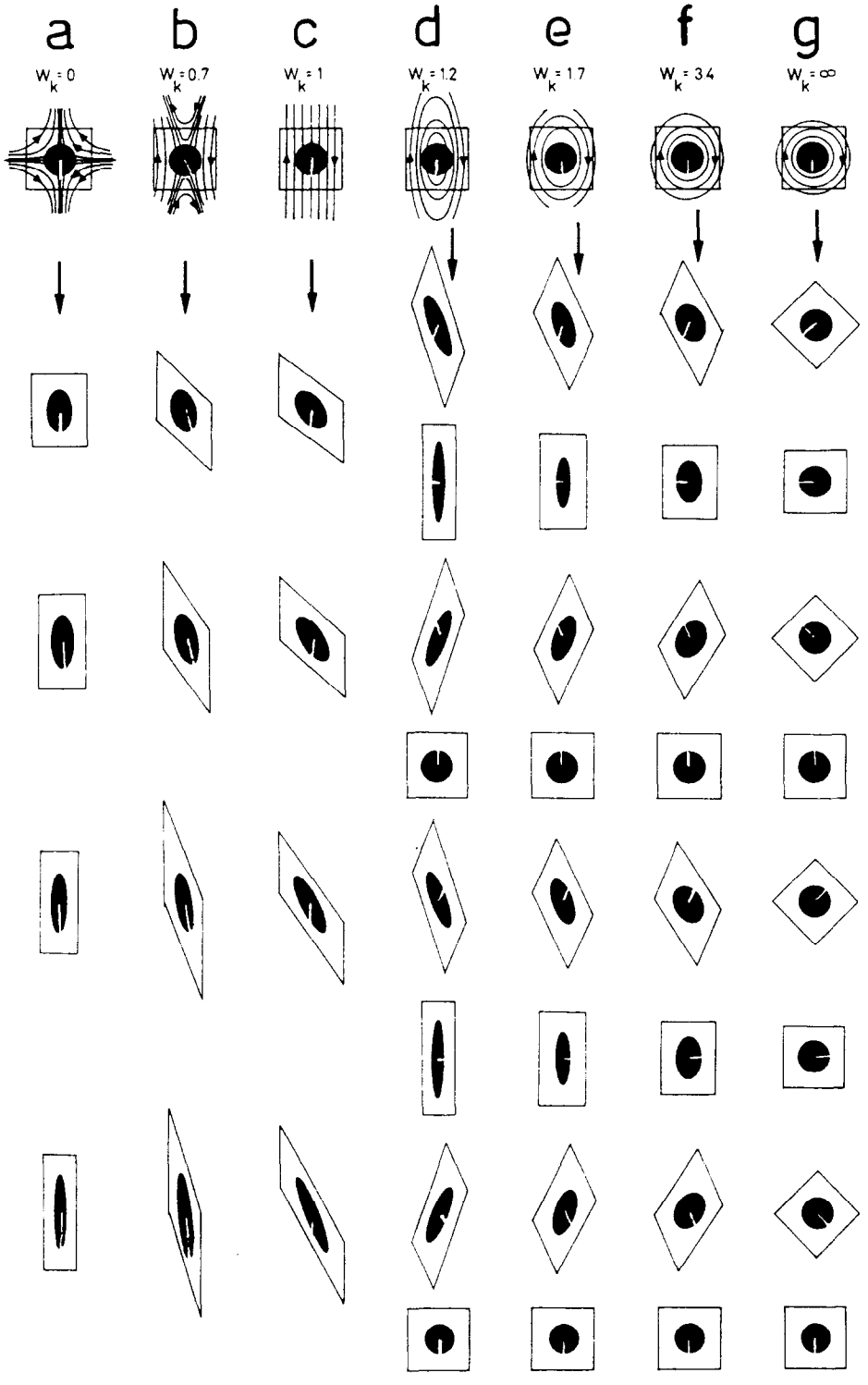


Fig. 1. Examples of homogeneous progressive deformation of passive strain markers in plane strain by the following particle movement paths (after Weijermars, 1988a): (a) pure shear deformation; (b) non-pulsating deformation with components of pure and simple shear superposed; (c) simple shear deformation; (d)–(f) pulsating strain; and (g) rigid-body rotation.

tion. Examples of the simultaneous visualization of particle movement paths and progressive deformation are shown here in physical laboratory experiments with a Taylor mill.

The progressive deformation of passive markers in pulsating and non-pulsating flow regimes in a Taylor mill obeys analytical expressions which relate the finite strain to the geometry of streamlines (and to a parameter for normalized time, see later, equations (5a)–(5d), (6a)–(6d)). However, methods to reconstruct streamlines or flowlines from deformation patterns observed in rocks are still limited. Particle movement paths occurring in rocks coincide with streamlines because inertia, which may cause a difference between particle movement paths

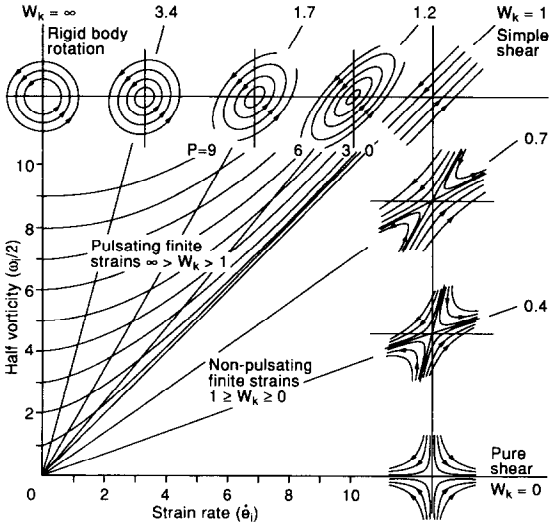


Fig. 2. Flow spectrum of homogeneous, plane flow, including those leading to pulsating and non-pulsating deformations. The occurrence of these flow paths critically depends on the kinematic vorticity number, $W_k$, the ratio of half the vorticity and the strain rate. Units along the axes are arbitrary and the frequency of pulsation, $P$, is in cycles per time unit (after Weijermars, 1988a).

Fig. 3. Overview of the Taylor mill used here.

and streamlines, is absent in solid-state creep of crystalline rocks (Weijermars and Schmeling, 1986). The differences and similarities between particle paths and streamlines (or flowlines) are concisely explained in basic textbooks on fluid mechanics (e.g. Tritton, 1988). In two-dimensional projections, any flowline represents a surface normal to the plane of view across which material transport does not occur. The flowline, thus, is part of an imaginary, impermeable surface. Some practical hints on ways to infer streamlines (or flowlines) from field structures are outlined in the final section of this paper.

## APPARATUS

The entire suite of two-dimensional flow patterns resulting in homogeneous plane deformation structures can be made visible in an elegant apparatus first designed in a study of the fluid mechanics of drop deformation and burst by Taylor (1879). Modern Taylor-mill designs have been made by Giesekus (1962), Fuller and Leal (1981) and Bentley and Leal (1986), the latter two also in connection with studies of drop burst. The four-roll mill built by Giesekus and used in his classical study (Giesekus, 1962) was kindly made available to the author. The apparatus comprises four rollers rotating about vertical axes causing flow in an ambient fluid. The flow patterns that are studied occur in the central space between the rollers (Fig. 3). The pattern of flow is principally controlled by the relative speed of the rollers and by their relative direction of rotation.

For the present study, the mill was refurbished with two independent electric motors and gearboxes. The four rollers each occupy a corner of an imaginary square (Fig. 4a–d). The ribs of the square are 95 mm apart, the radius of the rollers is 28 mm and the roller height is 56 mm. The rollers are mounted on a mobile frame which allows lowering of the rollers into a 250 × 250 × 50 mm Perspex container. The container is filled with glycerol, a transparent commercial fluid with density of 1261 kg $m^{-3}$, and a dynamic viscosity of 1 Pa s at 24°C. The four rollers are cross-wise coupled by rubber-belts, and each pair is driven by an independent electric motor. The motors were custom-made, and each of them is controlled by a 10-speed gearbox enabling selection of

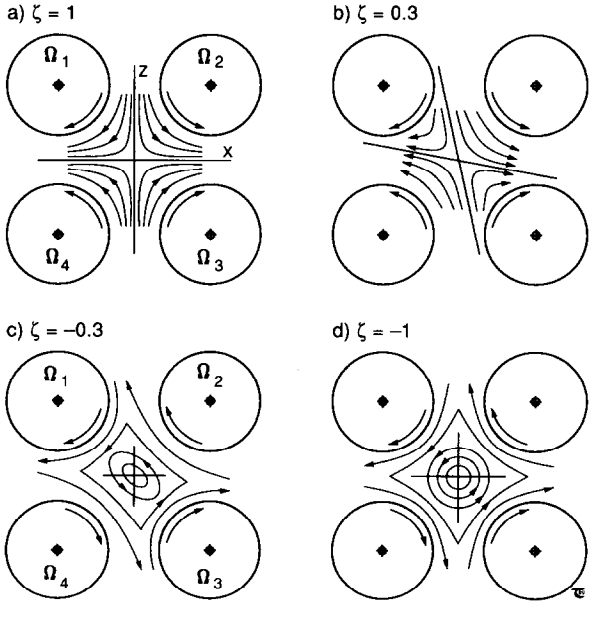


Fig. 4. Principle sketch of Taylor's four-roll mill in top view. Sense of roller rotation and their relative speed determines the geometry of the flowlines simulated: (a) pure shear; (b) oblique flow; (c) elliptical particle paths; and (d) rigid-body rotation.

integer rates between 1 and 10 rotations per min (rpm). The fluid container used in our study was illuminated from below by a 1000 W lamp and photographed from above by a tripod-mounted Nikon camera, loaded with Ektachrome 100 ASA daylight diapositive film, with shutter speed set at 1/250 s and diaphragm at 8. The flow was visualized using red and green dyes on a glycerol basis, commercially available as liquid food colourants. An alternative approach visualizes the flow by alignment of solid carbon particles suspended in the fluid, which yields flow patterns of a coarser resolution with no apparent instability near the stagnation points (Giesekus, 1962).

Figure 5(a–d) shows examples of the basic flow types observed in the Taylor mill by fixing the speed ratio of the four rollers (according to $\zeta$ in equation (2a) below) and adjusting the roller placement if necessary. Minor deviations from the ideal flow patterns occur near the central stagnation point of Fig. 5(a), where the dye lines in the direction of the shortening flow tend to fold, thus indicating that there exists a slight viscosity contrast between the various liquids used in the flow visualization. The dye lines in Fig. 5(a–d) closely follow the flowlines and were created by stretching dye markers, inserted by means of syringes.

The flow patterns produced in a Taylor mill can be characterized by the following stream function (Weijermars, 1991):

$$\psi = (\gamma/2)(z^2 - \zeta x^2) \tag{1}$$

where $\zeta$ is a dimensionless scaling parameter characterizing the flow pattern developing with shear strain rate $\gamma$. The coordinate system $ZX$ is as defined in Fig. 6(a). The scaling parameter $\zeta$ is controlled by the roller speeds (Bentley and Leal, 1986):

$$\zeta = -(\Omega_1 + \Omega_3)/(\Omega_2 + \Omega_4) \tag{2a}$$

with angular rotation rates $\Omega_1, ..., \Omega_4$ defined as in Fig. 4. Familiar cases of progressive deformation occur for $\zeta = -1$ (pure rotation and no strain, $W_k = \infty$), $\zeta = 0$ (simple shear, $W_k = 1$) and $\zeta = 1$ (pure shear, $W_k = 0$).

In the case of hyperbolic flowlines (Fig. 6a), typical for non-pulsating strains, $\zeta$ is related to the acute asymptote angle, $\alpha$, which is the angle between the flow apophyses (Fuller and Leal, 1981):

$$\zeta = \tan^2(\alpha/2) \tag{2b}$$

The major principal stress, $\tau_1$, in such flows is oriented at $2\alpha$ from the $X$-axis coinciding with one of the flow asymptotes or flow apophyses. In the case of elliptical flowlines (Fig. 6b), typical for pulsating strains, $\zeta$ is related to the axial ratio of the short and the long axis of elliptical streamlines (Fuller and Leal, 1981):

$$\zeta = -(b/a)^2 \tag{2c}$$

The scalar $\zeta$, used here to characterize particle movement paths, has been related to the kinematic vorticity number, $W_k$, elsewhere (Weijermars, 1991):

$$W_k = (1 - \zeta)/(1 + \zeta) \tag{3a}$$

The mathematical solution of $\zeta$ in terms of $W_k$ is:

$$\zeta = (1 - W_k)^2/(W_k^2 - 1) \tag{3b}$$

The major principal strain rate, $\dot{e}_1$, in each experiment can be obtained by measuring the velocity of the particles and substituting the observed velocities in the theoretical particle path equations. Once the strain rate is fixed, the finite strain after a particular time, $t$, can be calculated from the deformation tensor equations (5a)–(5d), (6a)–(6d) outlined below, using the normalized time $R_t (= \dot{e}_1 t)$. Various formulations for the particle path equations for *hyperbolic* flows are available from the literature: Giesekus (1962, equation 6), Ramberg (1975a, equation 38 or 1975b, equation 43), McKenzie (1979, equation 28), Fuller and Leal (1981, equation 16), Bentley and Leal (1986, equations 44 and 45) and Weijermars (1991, equations 15 and 16a–d). Similarly, *elliptical* particle path equations have been derived by Giesekus (1962, equation 10), Ramberg (1975a, equation 72 or 1975b, equation 52), McKenzie (1979, equation 30), Fuller and Leal (1981, equation 19) and Weijermars (1993b, equations 6 and 7a–d).

## DEFORMATION THEORY

The analytical expressions given below enable the computation of the finite strain and rotation of a strain ellipse after any arbitrary time of flow in a Taylor mill. The deformation tensor, $\boldsymbol{F}_{ij}$, if expressed in time-dependent terms, provides the parameters for a coordinate transformation describing the migrated positions, $x_i$, of material particles with initial positions, $x_j$:

$$x_i = \boldsymbol{F}_{ij} x_j \tag{4}$$

Attention is here confined to plane strains. If the coordinate system is fixed in an appropriate orientation (see later), only elements $F_{11}$, $F_{13}$, $F_{31}$ and $F_{33}$ may change during planar deformation (from initial unit length, representing undeformed self-projection of points), $F_{22}$ retains unit length, and all other tensor components remain zero at all times.

For the present purpose it is most practical to formulate the deformation tensor in terms of geometrical characteristics of the observed flow patterns. The deformation history for monotonically increasing strains is fully determined if the angle $\alpha$ between the two straight streamlines or flow asymptotes is known (Fig. 6a) (Weijermars and Poliakov, 1993):

$$F_{11} = \exp(R_t \sin \alpha) \tag{5a}$$

$$F_{13} = [\exp(R_t \sin \alpha) - \exp(-R_t \sin \alpha)] \cot \alpha \tag{5b}$$

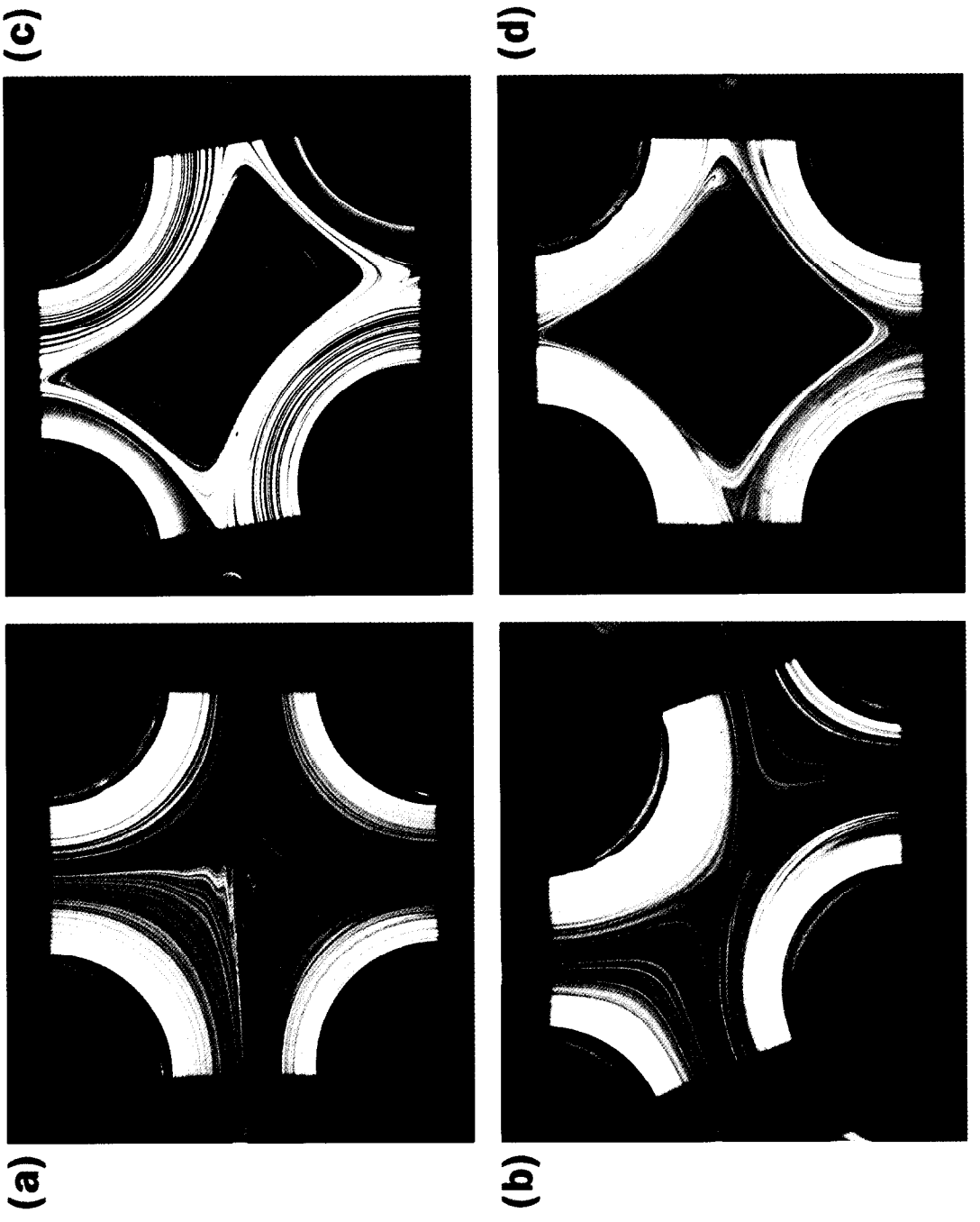


Fig. 5. Streamline patterns produced in a Taylor mill: (a) $\zeta = 1$ (pure shear, $W_k = 0$); (b) $\zeta = 0.5$ ($W_k = 0.33$); (c) $\zeta = -0.05$ (approx. simple shear, $W_k = 1.1$); and (d) $\zeta = -1$ (rigid-body rotation, $W_k = \infty$).

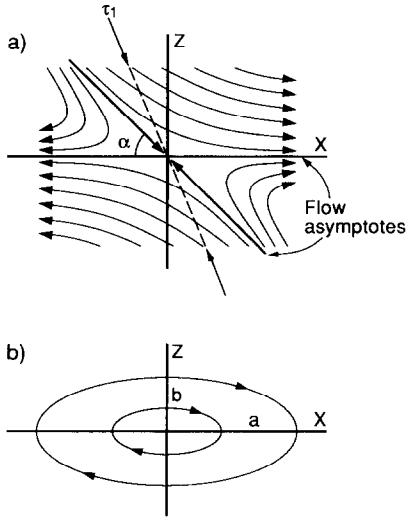


Fig. 6. The deformation tensor of flows valid for the coordinate systems as defined here can be determined directly from the flow geometry. (a) Monotonically increasing, homogeneous deformation paths can be characterized by the angle $\alpha$ between the two flow asymptotes (also termed flow apophyses). See equations (5a)–(5d). The orientation of the major principal stress axis, $\tau_1$, can also be related to $\alpha$ (see Table 1). (b) Pulsating strains are controlled by the ellipticity ($a/b$) of the streamlines. See equations (6a)–(6d).

$$F_{31} = 0 \tag{5c}$$

$$F_{33} = \exp(-R_t \sin \alpha) \tag{5d}$$

with the normalized time $R_t$ resulting from the product of principal strain rate, $\dot{e}_1$ (as determined from the experiment), and dimensional time, $t$. The deformation tensor elements of equations (5a)–(5d) are valid for a Cartesian coordinate system with the $X$-axis kept parallel to the exit flow asymptote, and the $Y$-axis perpendicular to the plane of flow which is in the $X$–$Z$ plane (Fig. 6a).

For pulsating or oscillating strains the progressive deformation of passive markers is also fully determinable from the normalized long axis of the elliptical streamlines, or simply the axial ratio $a/b$ (Fig. 6b) (adapted from Weijermars, 1993b):

$$F_{11} = \cos R_t \tag{6a}$$

$$F_{13} = (a/b) \sin R_t \tag{6b}$$

$$F_{31} = -(b/a) \sin R_t \tag{6c}$$

$$F_{33} = \cos R_t \tag{6d}$$

The physical meaning of the deformation tensor elements of equations (5a)–(5d), (6a)–(6d) is illustrated in Fig. 7(a & b) for a Cartesian coordinate system such as used in Fig. 6(a). Exactly the same dimensions occur for pulsating strains when the $X$-axis used in Fig. 7 coincides with the long axis of the elliptical streamline patterns, and the $Y$-axis remains perpendicular to the direction or plane of flow, which is in the $X$–$Z$ plane.

The stretch history of the long axis of an initial strain

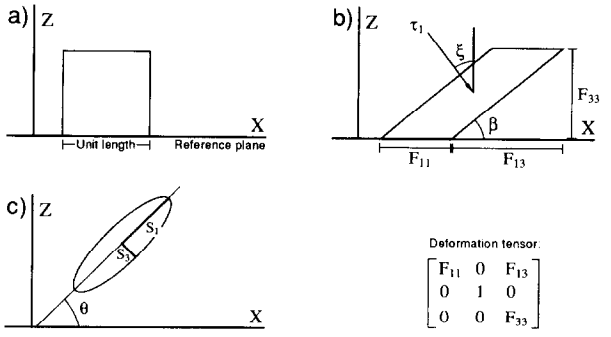


Fig. 7. Sketches illustrating how deformation tensor elements $F_{11}$, $F_{13}$ and $F_{33}$ relate to physical dimensions. See text for explanation.

circle (Fig. 7c) is given here in tensor notation, but has appeared in parameter form more than a century ago (Thompson and Tait, 1879):

$$S_1 = \left[0.5\left(K + \left[K^2 - 4(F_{11}F_{33} - F_{13}F_{31})^2\right]^{1/2}\right)\right]^{1/2} \tag{7a}$$

with $K = F_{11}^2 + F_{13}^2 + F_{31}^2 + F_{33}^2$ and tensor elements $F_{11}$, $F_{13}$, $F_{31}$ and $F_{33}$ (for details see Weijermars, 1991). The assumption of plane strain and no volume change implies that $S_3 = 1/S_1$. One can see that a rigid-body translation, which has tensor elements $F_{11} = F_{22} = F_{33} = 1$, and $F_{13} = 0$, yields a unit circle with $S_1 = S_3 = 1$.

The rotation history of the finite strain ellipse is also included in the deformation tensor. The orientation, at any time, is specified in terms of the angle $\theta$ between the finite strain ellipsoid's major axis and the $X$-axis (Fig. 7c):

$$\theta = 0.5 \arctan[(2F_{11}F_{31} - 2F_{13}F_{33})/(F_{11}^2 + F_{13}^2 - F_{31}^2 - F_{33}^2)]. \tag{7b}$$

Substitution of the $F_{ij}$ values for a unit simple shear, which has $F_{13} = 0$ and $F_{11} = F_{22} = F_{33} = 1$, and all other tensor components equal zero, yields $\theta = 31.7°$, confirming the validity of equation (7b).

## STRAIN VISUALIZATION

The basic flow configurations obtainable in the Taylor mill were subsequently used to visualize the progressive deformation of passive strain circles marked by a droplet of green dye in the centre of the flows. The sequential snapshots of Fig. 8(a) illustrate the progressive deformation of such a strain circle in a pure shear flow ($\zeta = 1$, $W_k = 0$). The strain ellipse stretches from 1 through to 1.4 to attain $S_1 = 2$ in the lowermost picture. Figure 8(b & c) visualizes the development of similar stretches in oblique shear flows characterized by $\zeta = 0.7$ ($W_k = 0.18$) and $\zeta = 0.5$ ($W_k = 0.33$), respectively. The green droplet was inserted with a syringe at the surface of the glycerine basin near the central stagnation point of the flow. The stagnation point was determined from the streamline patterns of Fig. 5(a–d); any material transport ceases

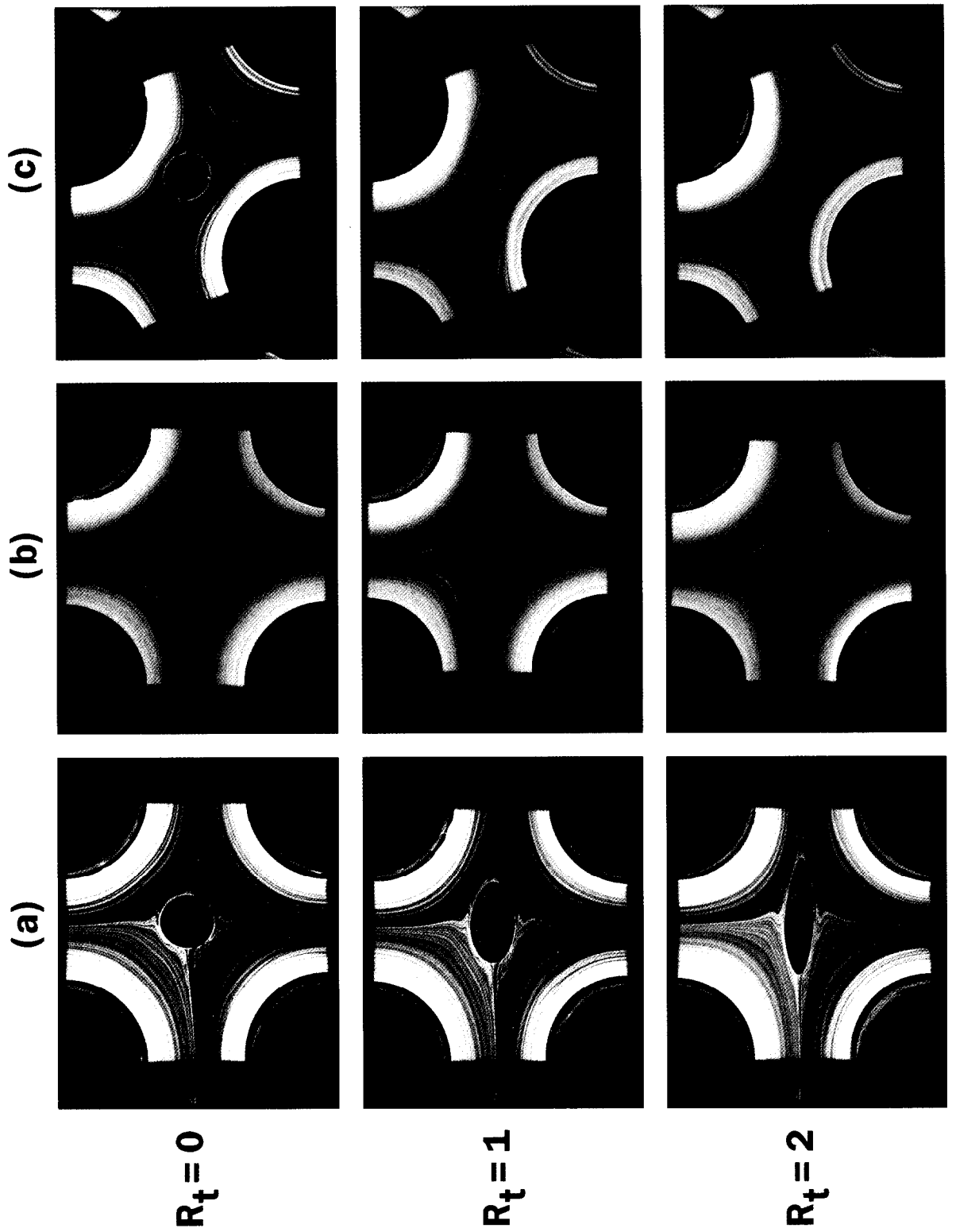


Fig. 8. Progressive deformation of an initial circle in the Taylor mill: (a) pure shear flow ($\zeta = 1$); (b) and (c) oblique shear flows characterized by $\zeta = 0.7$ ($W_k = 0.18$) and $\zeta = 0.5$ ($W_k = 0.33$), respectively. The strain ellipse stretches from 1 through to 1.4 to attain $S_1 = 2$ in the lowermost pictures.

immediately after stopping the rollers. A slight distortion of the pre-existing flowlines marked by the red dye occurred due to lateral spreading of the green droplet upon injection. Subsequently, the green marker was deformed after resuming the flow by switching the electric motors on again. Surface tension between the glycerol dyes and the ambient fluid is negligible. This could be inferred from the simple observation that green and red dyes stretch into infinitesimally thin lines *without* any droplet formation or failure. In contrast, surface tension was one of the critical parameters in the experiments by Bentley and Leal (1986), leading to droplet formation.

Figure 9(a) features sequential snapshots of an initially circular marker straining in the pulsating fashion described previously in theory only (Ramberg, 1975a,b; Pfiffner and Ramsay, 1982; Weijermars, 1993b, 1997a). The streamline pattern is characterized by $\zeta = -0.25$ ($W_k = 1.67$) and the maximum stretch is 1.45. The maximum stretch or ellipticity is aligned with the extensional asymptote of the flow. In rocks, this pulsating strain behaviour occurs in competent viscous inclusions, the maximum stretch being determined by the viscosity contrast between the inclusion and the host rock (Weijermars, 1993b, 1997a). Figure 9(b) effectively demonstrates rigid-body rotation or spin of a passive circular marker in the centre of circular streamlines with $\zeta = -1$ ($W_k = \infty$).

## DISCUSSION

The above experiments illustrate how material particles are transported along streamlines and how progressive, homogeneous deformation patterns result from such particle movements. The orientation of the flow asymptotes (or flow apophyses) in Taylor-mill experiments is controlled by the relative roller speed. There are no moving rollers inside deforming rocks, but rock particles deforming by surface stresses associated with displacing boundaries will follow similar streamlines if deforming homogeneously (Weijermars, 1993a). Although the particle movement paths themselves are not directly visible in deformed rocks, this section suggests methods to constrain the orientation of flow asymptotes from structures in deformed rocks. Mechanical analysis has previously demonstrated that elliptical particle paths cannot occur in rocks of isotropic bulk rheology flowing adjacent to a relatively rigid boundary (Weijermars, 1993b). Our attention, therefore, will focus on ways to reconstruct the orientation of the asymptotes of hyperbolic flows only.

The limiting assumptions made are: (1) homogeneous bulk deformation; (2) no volume change; and (3) plane deformation. It is sometimes inferred that fixed streamlines require an additional assumption of steady-state flow. This is not required as the flow rate may change over time. Nonetheless, the ratio of the vorticity and strain rate must remain fixed. This condition will automatically be fullfilled if the stress (or strain rate) axes remain stationary during the deformation. But the magnitude of the stress, strain rate and vorticity may all vary over time and thus need not be in steady state.

For hyperbolic flows associated with homogeneous bulk deformation, knowledge of the orientation of the two flow asymptotes defines the entire flow pattern (Fig. 6a). It is important to realize that the two flow asymptotes are different. One asymptote moves all particles toward the stagnation point of the flow (here termed the shortening flow asymptote). The other asymptote moves all particles away from the stagnation point (the extensional flow asymptote). Additionally, one of the two flow asymptotes is commonly parallel to the slip boundary fixed to the relatively rigid wallrock. If such a boundary can be identified, the orientation of the other asymptote follows if the angle $\alpha$ between them can be established by some of the field methods explained below.

Figure 10(a–e) illustrates the orientation of flow asymptotes in practical examples of single competent layers deforming in progressive deformation for a range of flows. The orientation of the extensional flow asymptotes is indicated in Fig. 10(a–e). The shortening flow asymptote is horizontal in Fig. 10(d & e), but oriented at $\alpha$ (equal to $\xi/2$), measured clockwise from the horizontal plane for the deformation in Fig. 10(a & b). The flow models of Fig. 10(a–e) assume a rigid boundary at the base of a deforming volume of rock. In a shear zone deforming by simple shear only, this concept of a rigid boundary is widely accepted. However, when the deformation deviates from simple shear it becomes more tenuous (e.g. Sanderson, 1973) and the differential shear has to be accommodated by a stretching fault (Means, 1989). One objection to the stretching fault concept is that faulting is unlikely to be coeval with ductile deformation required to form a grain shape fabric inside the shear zone. However, the stretching fault itself may well be a narrow zone of ductile shear. The amount of simple shear could vary laterally as the width of the stretching fault changes, in accordance with the observations by Simpson (1983). If the shear zone is *transpressional* (cf. Sanderson and Marchini, 1984), volume loss (e.g. by pressure solution) is likely to occur to help accommodate strain compatibility problems between the shear zone proper and the stable wallrock. Conversely, hydrothermal injection of rock matter such as quartz into dilating veins is likely to occur to solve strain compatibility problems in *transtensional* shear zones.

Figure 11(a–e) illustrates hyperbolic steady-state flow patterns mostly similar to those controlling the deformations in Fig. 10(a–e). In all these flows, one of the two flow asymptotes coincides with a stable boundary (here horizontal) adjacent to the deforming rock volume. Again, any differential slip at the boundary is accommodated by a stretching fault (Means, 1989). Grain shape fabrics, forming subparallel to the direction of maximum

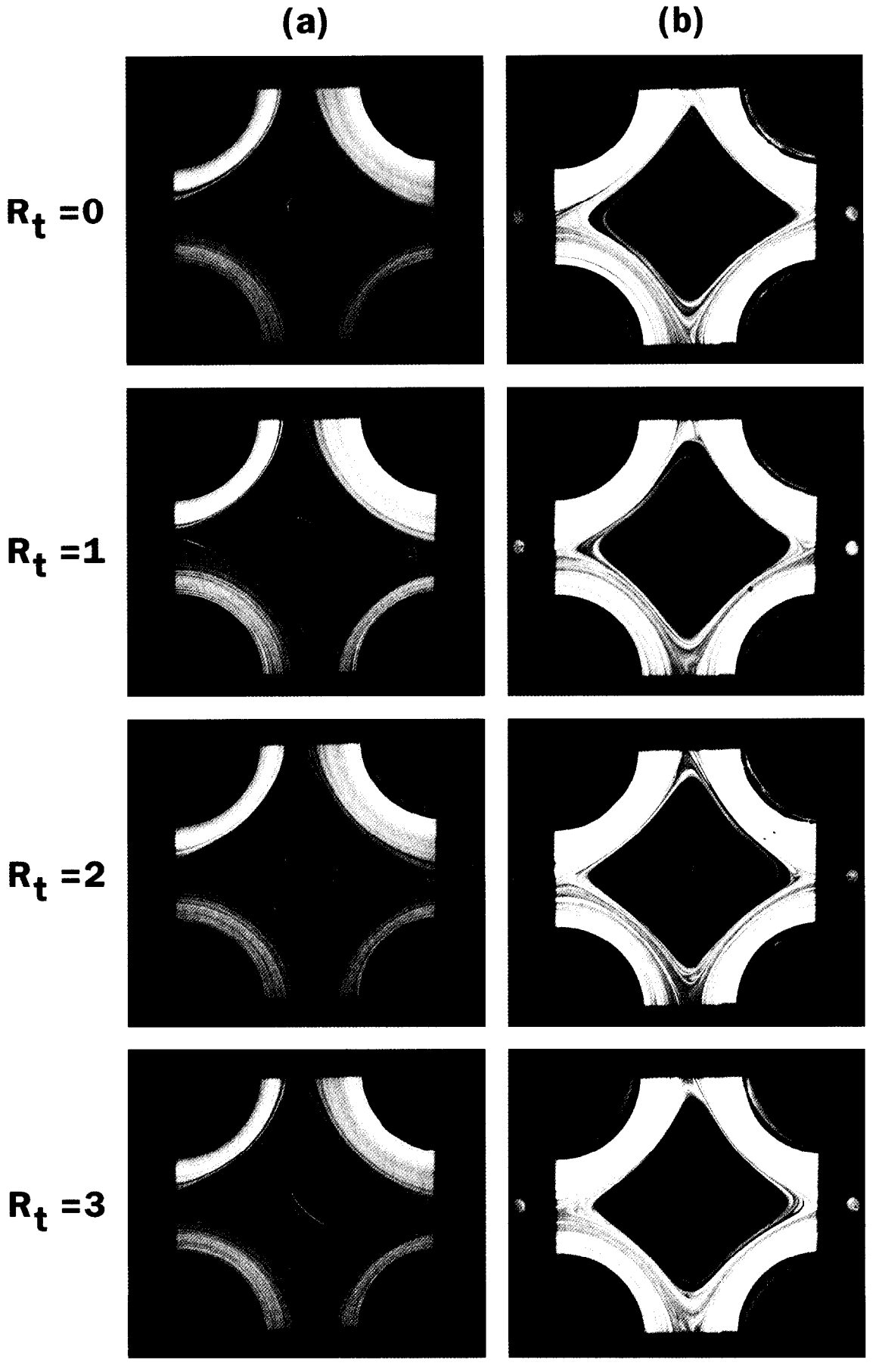


Fig. 9. Progressive deformation of initial circle in the Taylor mill: (a) elliptical particle paths with $\zeta = -0.25$ ($W_k = 1.67$) and the maximum stretch is 1.45; (b) effectively demonstrates rigid-body rotation or spin of a passive circular marker in the centre of circular streamlines with $\zeta = -1$ ($W_k = \infty$).

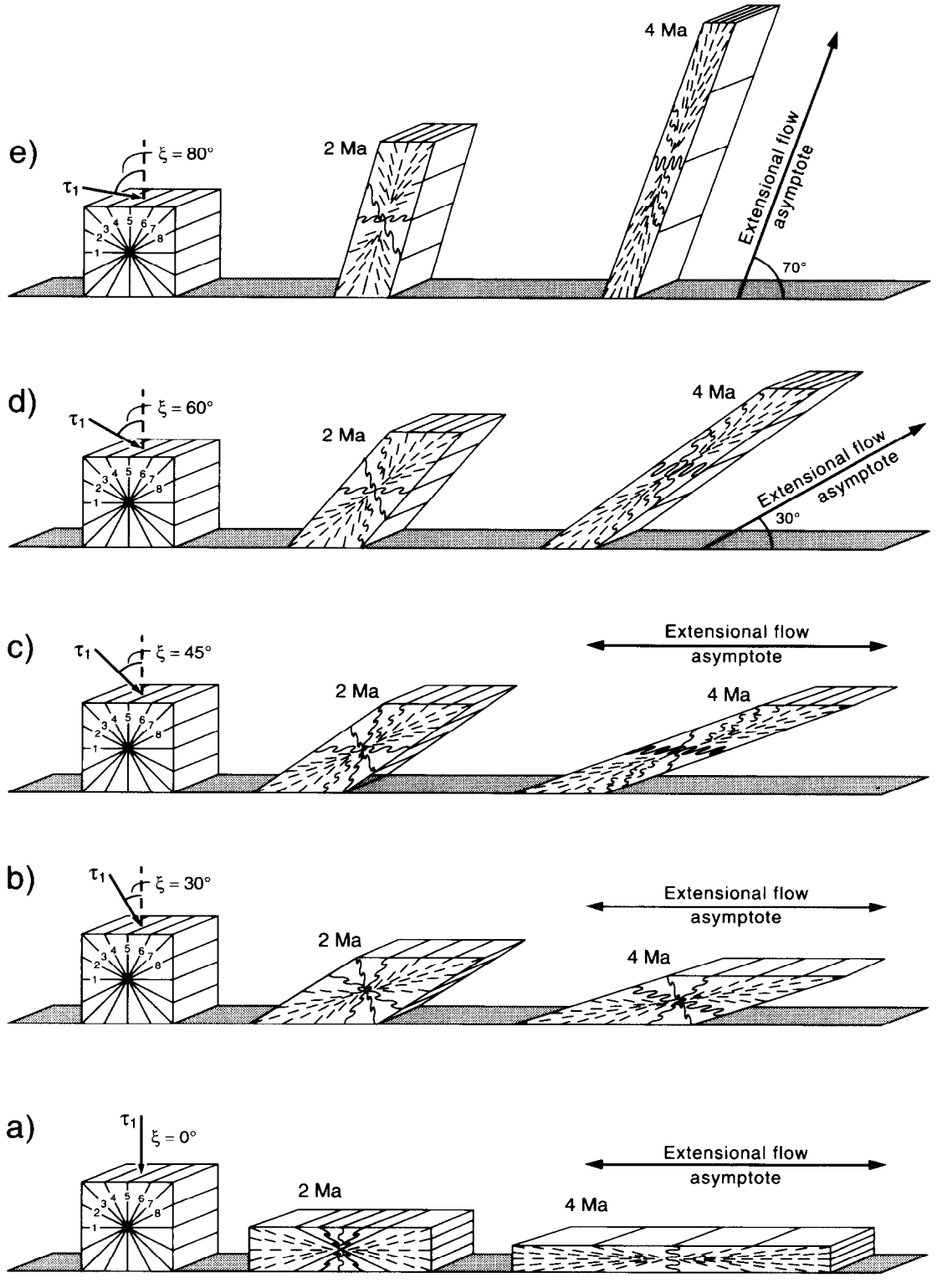


Fig. 10. Progressive deformation of a unit cube for the major principal stress orientations indicated. The boudinage and minor folds seen in the deforming blocks are for active, competent single layers. The stress magnitude and viscosity are such that a typical geological strain rate of $10^{-14}$ s$^{-1}$ occurs, with finite deformation patterns shown here at 2 Ma spacing (after Weijermars, 1993c). The orientation of the extensional flow asymptote is discussed in the text.

stretch as indicated by the extensional flow asymptotes, may further help to define the orientation of the second flow asymptote. Figure 11(a–c) illustrates a deformation zone that has either *thinned* or maintained a *constant thickness* during deformation. Thinning by *pure shear flow* ($\zeta = -1$ or $W_k = 0$) can be recognized from *symmetric* folds or *symmetric* mullions with the enveloping surface oriented perpendicular to the deformation zone

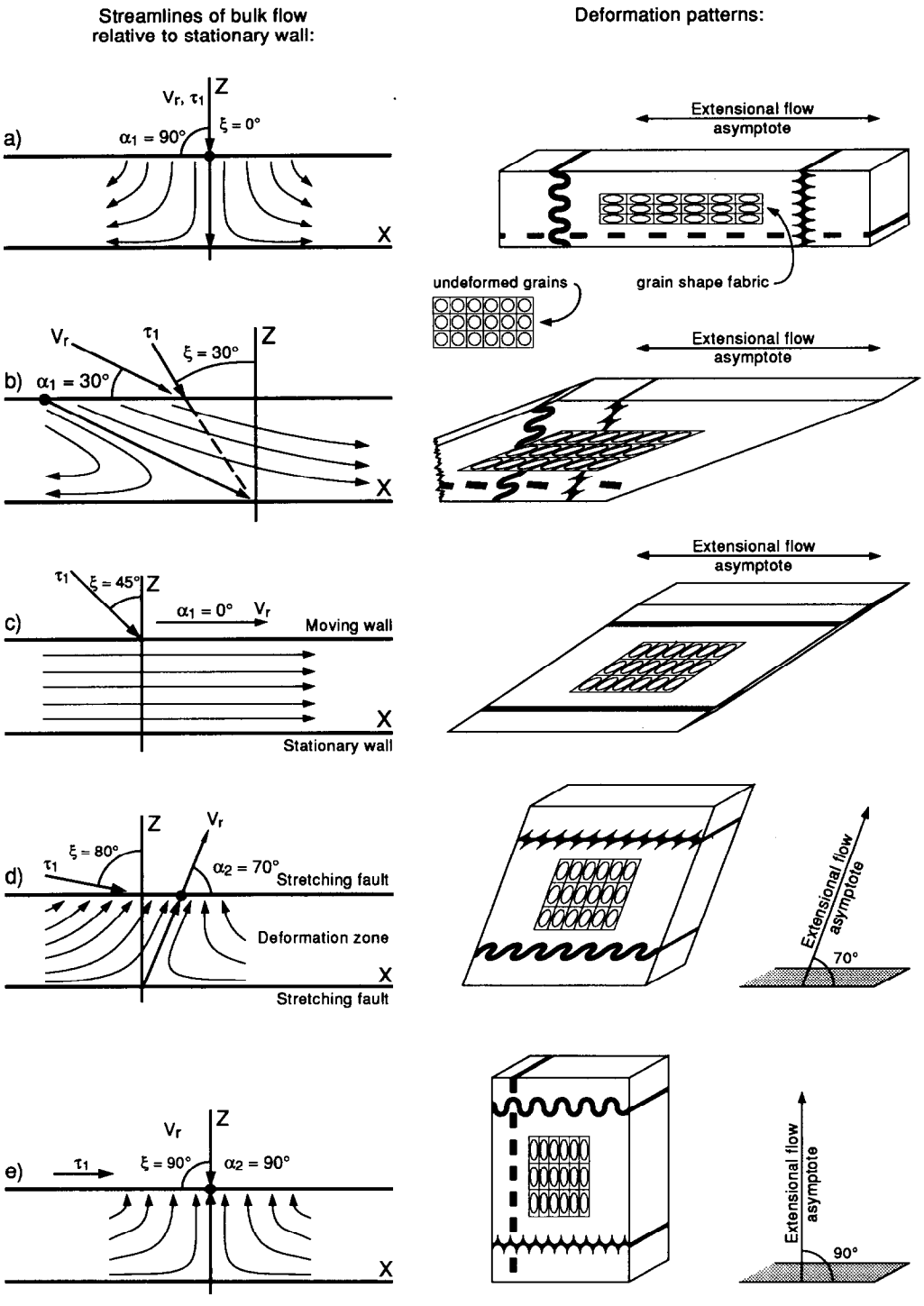


Fig. 11. Flowlines and associated homogeneous bulk deformation by the stress orientations $\xi = 0°$, 30°, 45°, 80°and 90° (i.e. $W_k = 0, 0.87, 1, 0.34$ and 0, as follows from $W_k = \sin 2\xi$, see Table 1). The structures indicated are for active, competent (folds, boudins) and incompetent (mullions) single layers. Finite strain portrayed as grain shape fabric is established after 3 Ma for a rock deforming at a strain rate of $10^{-14}$ s$^{-1}$. The direction of maximum stretch is parallel to the the stretching fault or the $X$-direction for principal deviatoric stress orientations $0° \leq \xi \leq 45°$. However, the direction of maximum stretch is not parallel to the $X$-axis but aligned with the orientation of the extensional flow asymptote for deformations where $45° < \xi \leq 90°$. The relative velocity vector, $\mathbf{V}_r$, of the upper boundary of the deforming volume is parallel to the inclined flow asymptotes.

boundaries (Fig. 11a). The tectonic foliation outlined by a grain shape fabric may be utilized to infer that the compressional flow asymptote has remained normal to the stable wallrock. *Simple shear* can be recognized if a competent or incompetent single layer parallel to the deformation zone boundaries has remained *undeformed*, because the material lines maintain constant length ($\zeta = 0$ or $W_k = 1$) (Fig. 11c). The angle between the two flow

Table 1. Conversion formulae for homogeneous two-dimensional flows and characteristic cases

| Parameter(s) | Kinematic vorticity number | Taylor-mill scaling parameter | Angle between flow asymptotes |
|---|---|---|---|
| Prefered symbol(s) | $W_k$ | $\zeta$ | $\alpha$ |
| Application | All planar flows | All planar flows | Hyperbolic flows |
| Special cases: | | | |
| Pure shear | 0 | 1 | 90° |
| Simple shear | 1 | 0 | 0° |
| Rigid-body rotation | $\infty$ | $-1$ | Not possible |
| Defined by | $W_k = \omega/2\dot{e}_1$ | $\zeta = (\Omega_1 + \Omega_3)/(\Omega_2 + \Omega_4)$ | $\alpha$ only |
| Required quantities | Vorticity ($\omega$), strain rate ($\dot{e}_1$) | Roller rotation rates ($\Omega_i$) | Angle between two flows asymptotes ($\alpha$) |
| Equivalence | $W_k = (1-\zeta)/(1+\zeta)$<br>$W_k = \cos\alpha$<br>$W_k = \sin 2\xi$<br>$W_k = (\eta_i/\eta_m)\sin 2\xi$<br>$W_k = \cos(\tan^{-1}[(\cot 2\xi)/\delta])$ | $\zeta = (1 - W_k)^2/(W_k^2 - 1)$<br>$\zeta = \tan^2(\alpha/2)$<br>$\zeta = -(b/a)^2$ | $\alpha = 90° - 2\xi$<br>$\alpha = \tan^{-1}[(\cot 2\xi)/\delta]$<br>$\alpha = 0.5\tan^{-1}(\zeta)^{1/2}$<br>$\alpha = \cos^{-1} W_k$ |
| Relationship with stream function,* $\psi(x, z)$ | $W_k = [(\partial^2\psi/\partial z^2) + (\partial^2\psi/\partial x^2)]/[(\partial^2\psi/\partial z^2) - (\partial^2\psi/\partial x^2)]$ | $\psi = (\gamma/2)(z^2 - \zeta x^2)$, with shear strain rate $\gamma$ | $\psi = \dot{e}_1(xz\sin\alpha + z^2\cos\alpha)$, with principal strain rate $\dot{e}_1$ |
| Sources | Truesdell, 1953; Means *et al.*, 1980; Weijermars, 1991 | Fuller and Leal, 1981; Bentley and Leal, 1986; Weijermars, 1991; this paper | Weijermars, 1991, 1993a; Weijermars and Poliakov, 1993 |

*For a specific flow orientation in Cartesian $XZ$ space.

asymptotes is effectively reduced to zero, so that they unite in the horizontal plane. The angle between the asymptotes of thinning flows intermediate between pure and simple shear ($-1 < \zeta < 0$ or $0 < W_k < 1$) can be further constrained using the deformation patterns of single competent layers of different orientations (Dennis and Secor, 1990; Weijermars, 1993c).

If the grain shape fabric is not parallel, but clearly inclined at angles larger than 45° to the boundaries of the deformation zone, it can be concluded that the deformation zone has *thickened* (Fig. 11d & e). Another assumption made here is that all grain shape fabrics will eventually rotate toward the plane occupied by the extensional flow asymptotes. This assumption is different to that of Sanderson (1974) and Coward (1980), who also argued that shear zones could deviate from simple shear but assumed that the grain shape fabrics studied record only a small increment of the deformation. Consequently, the long axis of the related strain ellipse had not rotated far away from the major infinitesimal stretching axis. In this study grain shapes are assumed to progressively rotate toward the infinitesimal stretching axis, as illustrated in Fig. 11(a–e). This also emphasizes that *foliation does not necessarily need to form normal to the major principal stress*, because the direction of maximum stretching is not always perpendicular to the major principal stress axis. The stress orientation in Fig. 11(a–e) is fixed as illustrated (Weijermars, 1993c).

Thickening by *pure shear flow* ($\zeta = -1$ or $W_k = 0$) can be inferred from symmetric folds or symmetric mullions with an enveloping surface oriented parallel to the boundaries of the deformation zone (Fig. 11e). The angle between the asymptotes of the thickening flows intermediate between pure and simple shear ($-1 < \zeta < 0$ or $0 < W_k < 1$) can be estimated by measuring the angle between the foliation trace and the stable boundary of the deformation zone. Strain fabrics are closely aligned to the extensional flow asymptote for such thickening flows. If the rocks are *strongly* foliated, then the foliation is likely to act as a mechanical anisotropy. This anisotropy forces foliated rocks to deform by simple shear flow in planes parallel to the anisotropy (Weijermars, 1992). If no foliation is present in the outcrop, asymmetric folds of single competent layers provide another possible source for determining the flow asymptote angle. The technique outlined here is adapted from a method for estimating the orientation of palaeostress axes using asymmetric folds adjacent to the Moroccan Border Fault (Weijermars, 1993a). Figure 7(a & b) illustrates how the normalized lengths of a deformed unit volume correspond to the deformation tensor components $F_{11}$, $F_{13}$ and $F_{33}$. Figure 12(a & b) outlines how these normalized lengths $F_{11}$, $F_{13}$ and $F_{33}$ can be determined for a practical situation involving asymmetric folds formed near a vertical detachment surface or stretching fault. $F_{11}$ follows by measuring the arc length $L_0$ of the folded competent layer, and subsequently normalizing the spacing, $L$, of axial planes as measured along the reference plane: $F_{11} = L/L_0$ (Fig. 12a). In general, folding of the competent layer only occurs if $F_{11} < 1$ and boudinage (not elaborated here) results if $F_{11} > 1$. $F_{13}$ may be calculated from $F_{11}$ and the angle, $\beta$, between the detachment surface and the axial plane, or any other rotated marker initially perpendicular to the detachment surface (Fig. 12b):

Table 1 (cont.). Conversion formulae for homogeneous two-dimensional flows and characteristic cases

| Orientation of major principal stress ($\tau_1$) | Ellipticity | Viscosity ratio and stress orientation | Anisotropy factor and orientation |
|---|---|---|---|
| $\xi$ | $a/b$ | $\eta_i/\eta_m$ and $\xi$ | $\delta$ and $\xi$ |
| Hyperbolic flows | Elliptical flows | Elliptical flows | Anisotropic flows |
| 0° and 90°<br>45°<br>Not possible | Not possible<br>$a/b=\infty$<br>$a/b=1$ | Not possible<br>$\eta_i/\eta_m=1$ and $\xi=45°$<br>$\eta_i/\eta_m \gg 1$ (or $\infty$) and $0°<\xi<90°$ | $\xi=0°$ or 90°, any $\delta$<br>$\delta \gg 1(\infty)$ and $0°<\xi<90°$<br>Not possible |
| $\xi$ only | $a/b$ | $\eta_i/\eta_m$ and $\xi$ | $\delta$ and $\xi$ |
| Angle ($\xi$) between $\tau_1$ and normal to stable boundary | Long axis ($a$), short axis ($b$) | Viscosity of inclusion ($\eta_i$) viscosity of matrix ($\eta_m$), stress angle ($\xi$) | Anisotropy factor ($\delta$) ($=\eta_S/\eta_N$), stress angle ($\xi$) |
| $\xi=45°-(\alpha/2)$<br>$\xi=0.5\sin^{-1} W_k$ | $a/b=[(\eta_i/\eta_m)+1]/[(\eta_i/\eta_m)^2-1)^{1/2}$ provided $\xi=45°$<br>$a/b=(W_k+1)/(W_k^2-1)^{1/2}$, provided $\xi=45°$ | $\eta_i/\eta_m=W_k$, provided $\xi=45°$ | $\delta=\cos 2\xi/[\tan(\cos^{-1} W_k)]$ |
| $\psi=\dot{e}_1(xz\cos 2\xi+z^2\sin 2\xi)$, with principal strain rate $\dot{e}_1$ | Not available | Not available | $\psi=(\tau_1/\eta_N)(xz\cos 2\xi+z^2\sin 2\xi)$, with normal viscosity $\eta_N$ |
| Weijermars, 1991 | Weijermars, 1993b, 1997a; this paper | Weijermars, 1993b, 1997a | Weijermars, 1992 |

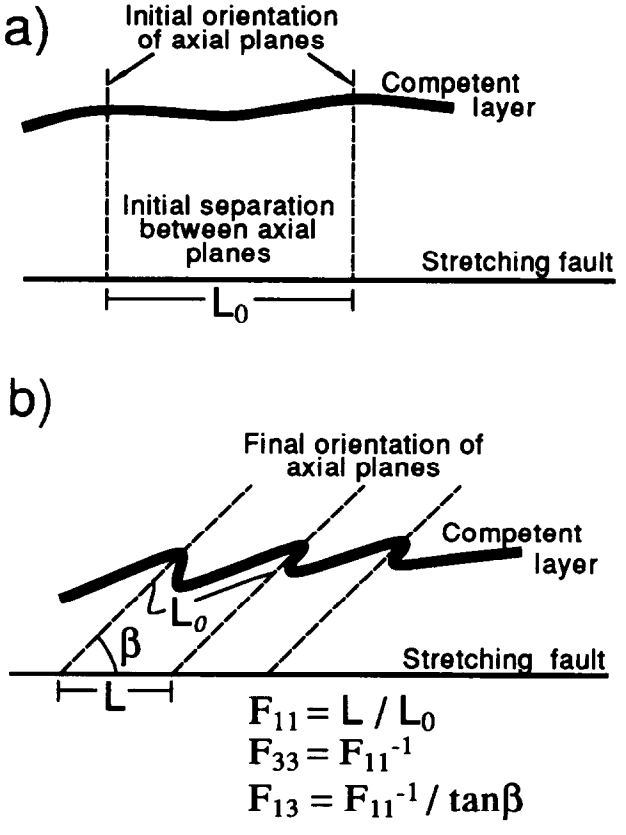


Fig. 12. Sketches explaining how the normalized lengths $L_0$ and $L$, the initial and final separation between axial planes, define the deformation tensor element $F_{11}$ ($=L/L_0$) portrayed as a physical length in Fig. 7(b). Deformation tensor element $F_{33}$ is equal to $F_{11}^{-1}$; $F_{13}$ follows from $F_{11}$ and angle $\beta$ through equation (8b). See text for an explanation.

$$\beta = \tan^{-1}(F_{11}^{-1}F_{13}^{-1}) \tag{8a}$$

$$F_{13} = F_{11}^{-1}/\tan\beta. \tag{8b}$$

Combining equation (5b) and equation (8b) yields an equation allowing the determination of the asymptote angle $\alpha$ using only $F_{11}$ and $\beta$:

$$\alpha = \arctan[(F_{11}^2 - 1)\tan\beta] + 180°, \text{ for } F_{11} < 1 \tag{9}$$

Recall that $F_{11}$ is measured as $L/L_0$ and together with $\beta$ can be measured as indicated in Fig. 12(b).

Rigid circular inclusions within the deformation zones where the bulk flow is hyperbolic can also help to infer the orientation of the asymptotes of the bulk flow pattern. Much detailed work on rigid inclusions has been published recently (Masuda and Ando, 1988; Bjornerud, 1989; Passchier *et al.*, 1993; Simpson and De Paor, 1993; Bjornerud and Zhang, 1995; Masuda *et al.*, 1995a,b; Ten Brink and Passchier, 1995; Masuda and Mizuno, 1996a,b), and the observations below are, of course, only complementary to that work. Figure 13(a–e) illustrates the same streamlines used in Fig. 11(a–e), but now in a reference frame fixed to the centre of a rigid inclusion inside the deformation zone. Such inclusions will encourage the development of either symmetric pressure shadows, or asymmetric winged porphyroblasts. Rigid inclusions remain stationary in pure shear deformation and pressure shadows around them are symmetric. However, if there is a component of simple shear involved in the deformation of the host rock ($W_k > 0$), the inclusions tend to rotate. The flow asymptotes will be

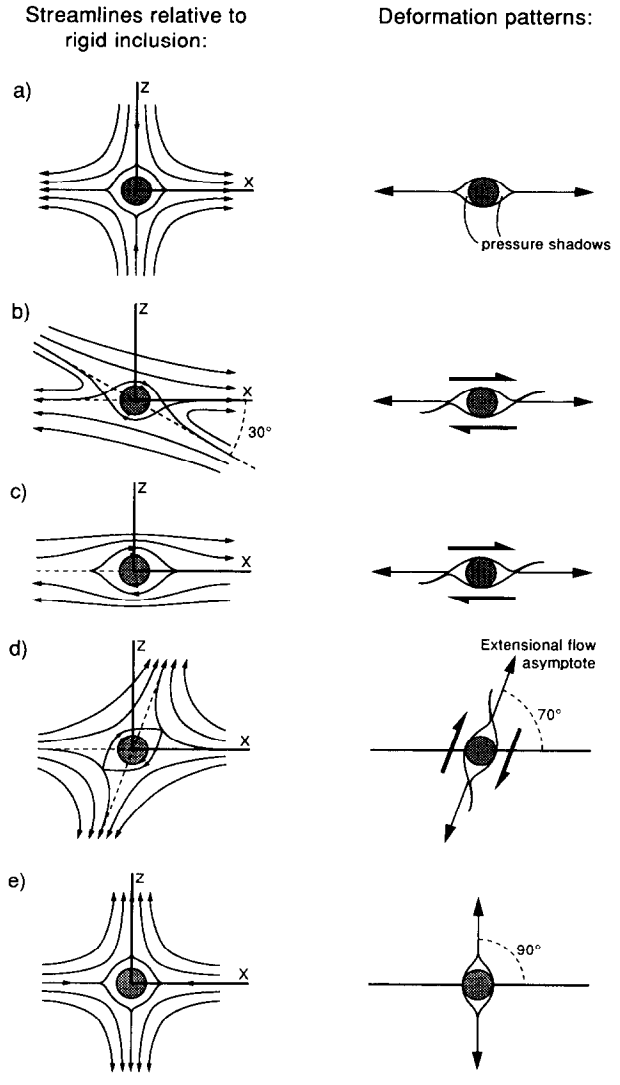


Fig. 13. Flowlines relative to rigid circular inclusions with cylinder axis parallel to the *Y*-direction. The bulk flow is similar to that portrayed in Fig. 11(a–e). Symmetric pressure shadows form for pure shear, and asymmetric wings are formed when a component of simple shear is involved. The axis of the pressure shadow is parallel to the extensional flow asymptote in all cases.

slightly curved near such inclusions (Fig. 13b), and the pressure shadows are typically asymmetric and can be used as kinematic indicators. The axis of the wings of the inclusions remain subparallel to the extensional flow asymptote, which may be either parallel to or inclined to the boundary of the deformation zone (Fig. 13b & d). The rate of rotation is fastest in simple shear, but the resulting asymmetry of the kinematic indicators (Fig. 13c) cannot be distinguished from those produced during flow involving components of pure shear (Fig. 13b & d). *However, any grain shape foliation aligning with the extensional flow asymptote is oblique to the boundary of the deformation zone if transtension has occurred* (Fig. 13d), *but parallel to the boundary for transpression* (Fig. 13b). The axis of the pressure shadows align with the extensional flow asymptote in all cases illustrated. For pure extension normal to the wall of the deformation zone (Fig. 13e), any grain shape fabric forms normal to the wall and thus helps to distinguish such zones of pure extension from pure shortening (Fig. 13a).

## CONCLUSIONS

The progressive deformation of passive markers in a Taylor-mill flow confirms the validity of analytical expressions that describe the progressive development of finite strains, using parameters based on the geometry of the streamlines (i.e. equations (5a)–(5d), (6a)–(6d)). In planar flows, one can distinguish between hyperbolic flow patterns and elliptical flow patterns. The hyperbolic flow patterns result in monotonically increasing finite strains. The elliptical flow patterns cause pulsating finite strains. Each flow pattern fixes the deformation history of a passive strain marker in a unique fashion. *Nomograms* that quantify the finite strain development for such flow patterns at normalized flow times ($R_t$) have been published in earlier work: for hyperbolic flows in isotropic media (Weijermars, 1991), for hyperbolic flows in anisotropic media (Weijermars, 1992), and for elliptical flows in two (Weijermars, 1993b) and three dimensions (Weijermars, 1997a).

The flow patterns themselves can be characterized concisely in several ways, using one of the following parameters or pairs of parameters: the kinematic vorticity number ($W_k$), the Taylor-mill scaling parameter ($\zeta$), the flow asymptote angle ($\alpha$, in hyperbolic flows only), the major principal stress axis orientation ($\xi$, in hyperbolic flows only), the ellipticity of the streamlines ($a/b$, in elliptical flows only), the viscosity ratio ($\eta_{inclusion}/\eta_{matrix}$, in elliptical flows only) and the anisotropy factor ($\delta$, in anisotropic flows only) together with the bulk stress orientation ($\xi$). Each of these different parameters may be useful for characterizing particular patterns of planar flow that guide homogeneous deformations. Table 1 compiles these dimensionless parameters for flow characterization according to various specific methods of flow engineering and aids the conversion between them. A more complete description of flows uses the stream function, and the relationship between the various parameters and the stream function is included in Table 1.

It can be concluded that theoretical and experimental knowledge of the relationship between flowline patterns and progressive deformation has progressed significantly. What urgently needs to be explored further is how we can reconstruct the flow patterns that have governed the development of deformation structures in rocks. Such flow patterns are not necessarily homogeneous, especially not if studying large-scale deformations. Also, such flows may be three-dimensional rather than two-dimensional with respect to flow symmetry. Many of the two-dimensional results can be easily extrapolated to three-dimensional flows (Weijermars, 1997a,b). Some hints for constraining two-dimensional

flow geometries from rock structures have been outlined in the preceeding Discussion section. Additional methods have been suggested elsewhere (Passchier and Simpson, 1986; Hanmer and Passchier, 1991; Simpson and De Paor, 1993; Jiang and White, 1995; Masuda *et al.*, 1995a,b; Tikoff and Fossen, 1995).

Finally, possibilities for future research on the basis of this study are as follows. Pure and simple shear boxes have been widely used in scaled and unscaled models of mechanical instabilities with geological significance (folds, mullions, boudins, etc.). The study of these shearing instabilities may be expanded by using robust designs of the Taylor flow apparatus, assembled with electromotors powerful enough to maintain flow in high viscosity polymers like the transparent SGM36 which is suitable for detailed strain studies (Weijermars, 1988b). The rheology of SGM36 and other polymers suitable for flow studies are documented in detail elsewhere (Weijermars, 1986a–c). The Taylor mill allows modelling, not only of pure and simple shear deformation, but of all possible cases of plane deformation. There are also new opportunities for modelling the deformation of inclusions of various shapes and a range of relative competence contrasts with the host material. In addition, the Taylor mill may be an excellent teaching aid in structural geology.

*Acknowledgements*—This work was supported by research grant ES/TRANS/154 of King Fahd University of Petroleum and Minerals. Professor Hans Giesekus provided generous help, hospitality and scientific encouragements at the University of Dortmund, January 1990. Refurbishment of the Giesekus design of the Taylor mill was accomplished at the Hans Ramberg Tectonic Laboratory, University of Uppsala, in 1991. Flow visualizations were photographed in 1992. Slides of the flow were presented at the Penrose conference on strain, Halifax, Nova Scotia, September 1993. Technical support was provided by Bertel Giös and Einar Meland, and funded by grants from the Swedish Natural Science Research Council (NFR).

## REFERENCES

Bentley, B. J. and Leal, L. G. (1986) A computer-controlled four-roll mill for investigations of particle and drop dynamics in two-dimensional linear shear flows. *Journal of Fluid Mechanics* **67**, 219–240.

Bjornerud, M. (1989) Mathematical model for folding of layering near rigid objects in shear deformation. *Journal of Structural Geology* **11**, 245–254.

Bjornerud, M. G. and Zhang, H. (1995) Flow mixing, object–matrix coherence, mantle growth and the developemnt of porphyroclast tails. *Journal of Structural Geology* **17**, 1347–1350.

Coward, M. P. (1980) The analysis of flow profiles in a basaltic dyke, using strained vesicles. *Journal of the Geological Society of London* **137**, 605–615.

Dennis, A. J. and Secor, D. T. (1990) On resolving shear direction in foliated rocks deformed by simple shear. *Bulletin of the Geological Society of America* **102**, 1257–1267.

Fuller, G. G. and Leal, L. G. (1981) Flow birefringence of concentrated polymer solutions in two-dimensional flows. *Journal of Polymer Science (Polymers Physical Edition)* **19**, 557–587.

Giesekus, H. (1962) Strömungen mit konstantem Geschwindigkeitsgradienten und die Bewegung von darin suspendierten Teilchen, Teil II: Ebene Strömungen und eine experimentelle Anordnung zu ihrer Realisierung. *Rheologica Acta*, Band 2, **2**, 112–122.

Hanmer, S. and Passchier, C. W. (1991) *Shear-sense Indicators: A Review*. Geological Survey of Canada Paper **90-17**.

Jiang, D. and White, J. C. (1995) Kinematics of rock flow and the interpretation of geological structures, with particular reference to shear zones. *Journal of Structural Geology* **17**, 1249–1266.

Masuda, T. and Ando, S. (1988) Viscous flow around a rigid spherical body: a hydrodynamical aproach. *Tectonophysics* **148**, 337–346.

Masuda, T., Michibayashi, K. and Otha, H. (1995a) Shape preferred orientation of rigid particles in a viscous matrix: re-evaluation to determine kinematic parameters of ductile deformation. *Journal of Structural Geology* **17**, 115–129.

Masuda, T., Mizuno, N., Kobayashi, M., Nam, T. N. and Otoh, S. (1995b) Stress and strain estimates for Newtonian and non-Newtonian materials in a rotational shear zone. *Journal of Structural Geology* **17**, 431–454.

Masuda, T. and Mizuno, N. (1996a) Deflection of non-Newtonian simple shear flow around a rigid cylindrical body by the Finite Element Method. *Journal of Structural Geology* **18**, 1089–1100.

Masuda, T. and Mizuno, N. (1996b) Computer modelling of mantled porphyroclasts in Newtonian and non-Newtonian simple shear viscous flows. *Journal of Structural Geology* **18**, 1487–1491.

Means, W. D. (1989) Stretching faults. *Geology* **17**, 893–896.

Means, W. D., Hobbs, B. E., Lister, G. S. and Willliams, P. F. (1980) Vorticity and non-coaxiallity in progressive deformation. *Journal of Structural Geology* **2**, 371–378.

McKenzie, D. P. (1979) Finite deformation during fluid flow. *Geophysical Journal of the Royal Astronomical Society* **59**, 689–715.

Passchier, C. W. and Simpson, C. (1986) Porphyroblast systems as kinematic indicators. *Journal of Structural Geology* **8**, 831–844.

Passchier, C. W., Ten Brink, C. E., Bons, P. D. and Sokoutis, D. (1993) $\delta$ objects as a gauge for stress sensitivity of strain rate in mylonite. *Earth and Planetary Science Letters* **120**, 239–245.

Pfiffner, A. O. and Ramsay, J. G. (1982) Constraints on geological strain rates: arguments from finite strain rates of naturally deformed rocks. *Journal of Geophysical Research* **87**, 311–321.

Ramberg, H. (1975a) Particle paths, displacement and progressive strain applicable to rocks. *Tectonophysics* **28**, 1–37; correction in *Tectonophysics* **121**, 355 (1986).

Ramberg, H. (1975b) Superposition of homogeneous strain and progressive deformation in rocks. *Bulletin of the Geological Institute, University of Uppsala, New Series* **6**, 35–67.

Sanderson, D. J. (1973) Models of strain variation in nappes and thrust sheets: a review. *Tectonophysics* **137**, 289–302.

Sanderson, D. J. (1974) Patterns of boudinage and apparent stretching lineation developed in folded rocks. *Journal of Geology* **82**, 651–661.

Sanderson, D. J. and Marchini, W. R. D. (1984) Transpression. *Journal of Structural Geology* **6**, 449–458.

Simpson, C. (1983) Displacement and strain patterns from naturally occurring shear zone terminations. *Journal of Structural Geology* **5**, 497–505.

Simpson, C. and De Paor, D. G. (1993) Strain and kinematic analysis in general shear zones. *Journal of Structural Geology* **15**, 1–20.

Taylor, G. F. (1879) The formation of emulsions in definable fields of flow. *Proceedings of the Royal Society, London* **29**, part 71, 501–523.

Ten Brink, C. E. and Passchier, C. W. (1995) Modelling of mantled porphyroclasts using non-Newtonian rock analogue materials. *Journal of Structural Geology* **17**, 131–146.

Thompson, W. and Tait, P. G. (1879) *Principles of Mechanics and Dynamics*, Part 1 (paperback version published, 1962). Dover, New York.

Tikoff, B. and Fossen, H. (1995) The limitations of three-dimensional kinematic vorticity analysis. *Journal of Structural Geology* **17**, 1771–1784.

Tritton, D. J. (1988) *Physical Fluid Dynamics* (2nd edn). Clarendon Press, Oxford.

Truesdell, C. (1953) Two measures of vorticity. *Journal of Rational Mechanical Analysis* **2**, 173–217.

Weijermars, R. (1986a) Polydimethylsiloxane flow defined for experiments in fluid dynamics. *Applied Physics Letters* **48**, 109–111.

Weijermars, R. (1986b) Finite strain of laminar flows can be visualized in SGM36-polymer. *Naturwissenschaften* **73**, 33–34.

Weijermars, R. (1986c) Flow behavior and physical chemistry of Bouncing Putties and related polymers in view of tectonic laboratory applications. *Tectonophysics* **124**, 325–358.

Weijermars, R. (1988a) Progressive deformation in low Reynolds number flow past a falling cylinder. *American Journal of Physics* **56**, 534–540.

Weijermars, R. (1988b) New laboratory method for analyzing deformation and displacement in creeping fluid: Examples from Stokes flow and a thermal plume. *Journal of Geophysical Research* **93**, 21279–21290.

Weijermars, R. (1991) The role of stress in ductile deformation. *Journal of Structural Geology* **13**, 1061–1078.

Weijermars, R. (1992) Progressive deformation in anisotropic rocks. *Journal of Structural Geology* **14**, 723–742.

Weijermars, R. (1993a) Estimation of palaeostress orientation within deformation zone between two mobile plates. *Bulletin of the Geological Society of America* **105**, 1491–1510.

Weijermars, R. (1993b) Pulsating strains. *Tectonophysics* **220**, 51–67.

Weijermars, R. (1993c) Progressive deformation of single layers under constantly oriented boundary stresses. *Journal of Structural Geology* **15**, 911 922.

Weijermars, R. (1997a) Pulsating oblate and prolate three-dimensional strains. *Mathematical Geology* **29**(1), 17–41.

Weijermars, R. (1997b) *Principles of Rock Mechanics*. Alboran Science Publishing, Amsterdam.

Weijermars, R. and Poliakov, A. (1993) Stream functions and complex potentials: Implications for development of rock fabric and the continuum assumption. *Tectonophysics* **220**, 33–50.

Weijermars, R. and Schmeling, H. (1986) Scaling of Newtonian and non-Newtonian fluid dynamics without inertia for quantitative modelling of rock flow due to gravity (including the concept of rheological similarity). *Physics of the Earth and Planetary Interiors* **43**, 316–330.